American Mineralogist, Volume 95, pages 19–23, 2010

Anisotropic elasticity of jarosite: A high-*P* synchrotron XRD study

Hongwu Xu,[1,*] Yusheng Zhao,[2] Jianzhong Zhang,[2] Yuejian Wang,[2] Donald D. Hickmott,[1] Luke L. Daemen,[2] Monika A. Hartl,[2] and Liping Wang[3]

[1]Earth and Environmental Sciences Division, Los Alamos National Laboratory, Los Alamos, New Mexico 87545, U.S.A.
[2]Los Alamos Neutron Science Center, Los Alamos National Laboratory, Los Alamos, New Mexico 87545, U.S.A.
[3]Department of Geosciences, State University of New York at Stony Brook, Stony Brook, New York 11794, U.S.A.

Abstract

The elastic properties of jarosite were investigated using synchrotron X-ray diffraction coupled with a multi-anvil apparatus at pressures up to 8.1 GPa. With increasing pressure, the *c* dimension contracts much more rapidly than *a*, resulting in a large anisotropy in compression. This behavior is consistent with the layered nature of the jarosite structure, in which the (001) $[Fe(O,OH)_6]/[SO_4]$ sheets are held together via relatively weak K-O and hydrogen bonds. Fitting of the measured unit-cell parameters to the second-order Birch-Murnaghan equation of state yielded a bulk modulus of 55.7 ± 1.4 GPa and zero-pressure linear compressibilities of 3.2×10^{-3} GPa^{-1} for the *a* axis and 13.6×10^{-3} GPa^{-1} for the *c* axis. These parameters represent the first experimental determination of the elastic properties of jarosite.

Keywords: Jarosite, elastic properties, compressibility, bulk modulus, equation of state, synchrotron X-ray diffraction

Introduction

Jarosite, $KFe_3(SO_4)_2(OH)_6$, a layered sulfate compound, has attracted considerable attention for several reasons. First, jarosite is a model antiferromagnetic compound for studying spin frustrations in two-dimensional *kagomé* lattices (composed of magnetic ions such as Fe^{3+} located at the corners of triangles that are linked via corner-sharing) (Wills et al. 2000). Second, jarosite is an important sulfate mineral. It occurs in acid mine drainage environments, as a weathering product of sulfide ore deposits, and can precipitate from aqueous sulfate in epithermal environments and hot springs associated with volcanic activity (Papike et al. 2006). In 2004, jarosite was detected by the Mars Exploration Rover (MER) Mössbauer spectrometer (Klingelhöfer et al. 2004), and it has been interpreted as strong evidence for the occurrence of large amounts of water (and possibly life) in the history of Mars (Kotler et al. 2008). Last, jarosite has industrial applications. In the Zn industry, precipitation of jarosite is an effective means to extract Fe impurities from Zn-sulfide ores (Dutrizac and Jambor 2000). In addition, jarosite and its associated alunite-type phases are potential hosts for long-term immobilization of radioactive fission products and toxic heavy metals (Ballhorn et al. 1989; Kolitsch et al. 1999).

Owing to its diverse applications, the structure and properties of jarosite have been extensively studied. The jarosite structure consists of $[SO_4]$ tetrahedra and distorted $[Fe(O,OH)_6]$ octahedra with K situated in a 12-fold-coordinated site (space group $R\bar{3}m$) (Fig. 1) (Menchetti and Sabelli 1976; Stoffregen et al. 2000; Basciano and Peterson 2007; Glasnak and Majzlan 2007). Each $[Fe(O,OH)_6]$ octahedron is linked to four $[Fe(O,OH)_6]$ octahedra in the (001) plane via OH-corner sharing and two $[SO_4]$ tetrahedra [one above the (001) plane and one below] via O-corner sharing, thereby forming $[Fe(O,OH)_6]/[SO_4]$ sheets perpendicular to the *c* axis. Potassium cations are located between the (001) $[Fe(O,OH)_6]/[SO_4]$ sheets with each K being coordinated to six O atoms [from (SO_4) tetrahedra] and six OH groups {from $[Fe(O,OH)_6]$ octahedra}. The unique distribution of magnetic Fe^{3+} ions within the (001) sheets of jarosite results in its interesting magnetic structure and properties. Neutron diffraction experiments reveal that jarosite exhibits long-range magnetic ordering when cooled below 65 K, as evidenced by the appearance of magnetic reflections at *hkl*/2, *l* = odd (Inami et al. 2000). This magnetic ordering is interpreted to result from the coupling between the jarosite (001) sheets exhibiting a net magnetization, which is mainly due to Dzyaloshinsky-Moriya (DM) anisotropic interactions (Grohol et al. 2003; Yildirim and Harris 2006).

Despite the detailed characterization of the structure and properties of jarosite at room and low temperatures, no information is available concerning its high-pressure behavior. The recent discovery of jarosite on Mars has spurred interests in its stability and structural behavior at various pressures, temperatures, and aqueous conditions (such as pH) (e.g., Drouet and Navrotsky 2003; Navrotsky et al. 2005). This information is also valuable for better utilization of jarosite as an Fe-impurity extractor in the Zn industry and as a potential host for radioactive/toxic wastes. In this study, we carried out in situ X-ray diffraction (XRD) experiments on jarosite using energy-dispersive synchrotron X-rays coupled with a multi-anvil press at pressures up to 8.1 GPa. Our experiments show that jarosite is stable up to the highest pressure achieved. Unit-cell parameters have been measured as function of pressure, and from these, axial and volume bulk moduli (compressibilities) have been determined for the first time. Our results reveal that the *c* axis exhibits a much larger compressibility than the *a* axis, and this anisotropy is consistent with the layered nature of the jarosite structure.

* E-mail: hxu@lanl.gov

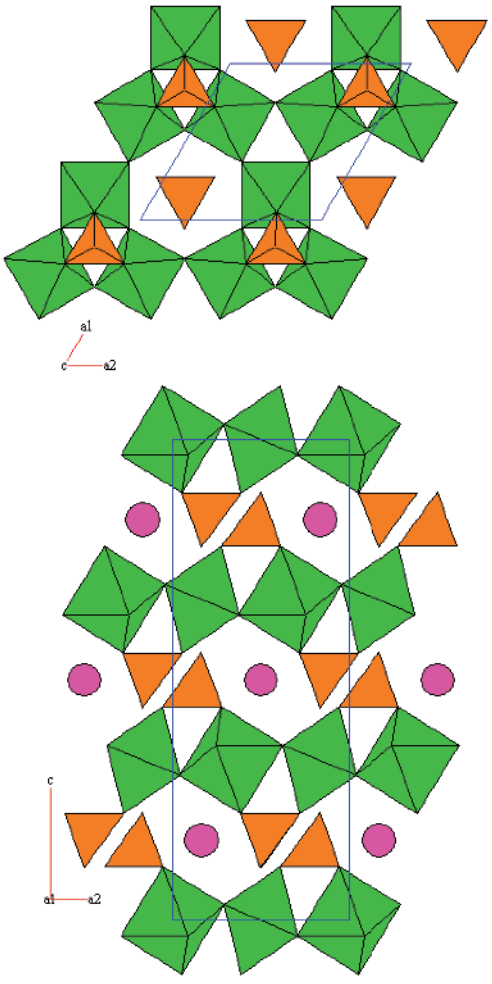

FIGURE 1. Structure of jarosite, $KFe_3(SO_4)_2(OH)_6$, projected along (**a**) the *c* axis and (**b**) the *a* axis. Brown tetrahedra represent $[SO_4]$ units, green octahedra represent $[Fe(O,OH)_6]$ units, and pink balls represent K. Blue lines outline the unit cell.

EXPERIMENTAL METHODS

We used a deuterated jarosite sample $[KFe_3(SO_4)_2(OD)_6]$ prepared via hydrothermal reaction of $Fe(NO_3)_3 \cdot 9D_2O$ and K_2SO_4 at 433 K for three days. It is the same sample as that used by Xu et al. (2009) in their high-temperature neutron diffraction study, where sample deuteration was needed to avoid large incoherent scattering of neutrons by hydrogen. Powder XRD, thermogravimetry, and chemical analysis confirmed the purity and stoichiometry of the sample (Xu et al. 2009).

Synchrotron XRD experiments were performed using energy-dispersive X-ray radiation from the superconducting wiggler magnet at beamline X17B2 of the National Synchrotron Light Source (NSLS), Brookhaven National Laboratory. The incident X-ray beam was collimated to dimensions of 100 × 100 μm, and the diffracted beams were collected with a solid Ge detector at a fixed angle of 2θ = 6.470°. The cell assembly used is similar to the DIA-type cells described by Weidner et al. (1992). Briefly, a mixture of amorphous boron and epoxy resin was utilized as the pressure-transmitting medium, and amorphous carbon as the furnace material. The powdered samples of jarosite and NaCl, the latter of which served as a pressure marker, were packed as separate layers into a cylindrical container of boron nitride, 1 mm in diameter and 2 mm in length. Pressure was calculated from Decker's equation of state for NaCl (Decker 1971) using the lattice parameter determined from the XRD pattern of NaCl at each experimental condition. Four diffraction peaks of NaCl—(200), (220), (222), and (420)—were used for determination of its lattice parameter. The uncertainties in the pressure measurements are mainly due to statistical variation in the positions of diffraction peaks and are between 0.1–0.2 GPa in the pressure range of this study. The experiments were carried out as follows: the sample was gradually compressed to 8.1 GPa, followed by decompression to 7.4, 6.5, 5.9, 4.7, 3.5, 2.1, and 1.1 GPa and room pressure. To decrease the deviatoric stress accumulated during compression, the sample/NaCl was heated to ~500 K at each pressure for a few minutes and then quenched to room temperature. Collection of XRD patterns started ~1 min thereafter.

RESULTS AND DISCUSSION

Our in-situ synchrotron XRD experiments show that jarosite is stable up to 8.1 GPa, the highest pressure used (Fig. 2). On compression, diffraction peaks become somewhat broadened and intensities drop significantly. This behavior is apparently due to the residual deviatoric stresses that were not released during the annealing at 500 K. Using the peak profile analysis method of Zhao and Zhang (2008) and based on a Young's modulus of 106.3 GPa for jarosite (calculated from the shear modulus and Poisson's ratio of Majzlan et al. 2006), the microscopic deviatoric stresses at 4.7 and 8.1 GPa were estimated to be 0.58 and 1.2 GPa, respectively [compared with a macroscopic differential stress of about 0.1 GPa for NaCl at 6 GPa and 500 K (Weidner et al. 1994)]. Annealing at a higher temperature may help relax these stresses. However, since jarosite starts to decompose into yavapaiite and hematite (as well as water vapor) at 575 K and room pressure (Xu et al. 2009), we did not use a higher annealing temperature. Thus, the sample was not under an optimal hydrostatic condition. Rather, it was probably in a semi-hydrostatic state. In addition, different diffraction peaks of jarosite show different magnitudes in their shifts to lower *d*-spacings or higher energies on compression. For instance, the (113) peak shifts more than the (021) peak. As a result, these

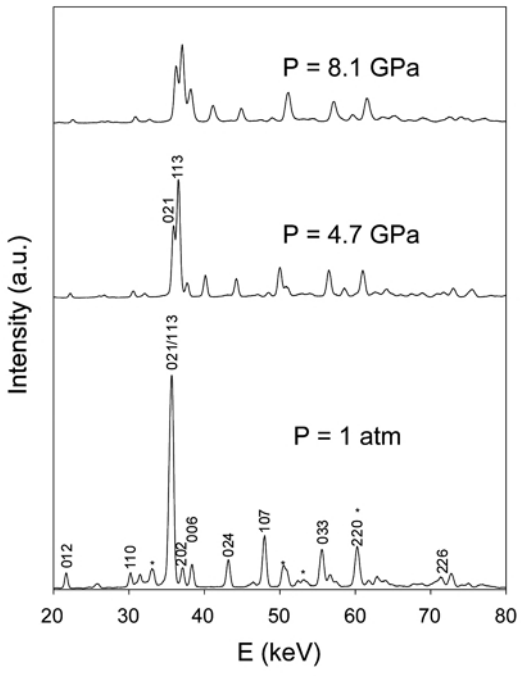

FIGURE 2. Selected synchrotron XRD patterns of jarosite at ambient condition, 4.7 and 8.1 GPa. Major jarosite peaks are labeled with their *hkl* indices, and stars indicate peaks from the boron nitride container.

two overlapped peaks at room pressure become separated at high pressure, and their separation increases with increasing pressure (Fig. 2). This behavior apparently reflects the anisotropic nature of the jarosite contraction (see below).

To obtain the bulk modulus (K_0) or compressibility (β_V, where $\beta_V = 1/K_0$) of jarosite, we determined its unit-cell parameters as a function of pressure. Diffraction peaks were fitted using the Plot85 program, and the cell parameters were determined from least-squares analyses of *d*-spacings of ten peaks: (012), (110), (021), (113), (202), (006), (024), (107), (033), and (220). The determined unit-cell parameters are listed in Table 1 and plotted in Figure 3. As shown in Figure 3, with increasing pressure, both *a* and *c* decrease, and thus cell volume, *V*, also decreases. Fitting the volume data to a second-order Birch-Murnaghan equation of state (EOS) (Birch 1952):

$$P = 1.5K_0 [(V_0/V)^{7/3} - (V_0/V)^{5/3}] \quad (1)$$

yielded a zero-pressure volume V_0 of 795.1(1.4) Å^3 and a bulk modulus K_0 of 55.7(1.4) GPa. The fit is good, as reflected by an R^2 value of 0.997 and that the fitted V_0 is essentially the same as the measured V_0 at room pressure (794.6 ± 0.4 Å^3). The pressure derivative of the bulk modulus K_0' (=$\partial K_0/\partial$P) was fixed at 4.0, a reasonably estimated K_0' value for most materials. Indeed, our *f*-*F* analysis (*f* is the Eulerian strain and *F* the normalized stress) confirmed that the *P*-*V* data can adequately be fitted with a second-order truncation of the Birch-Murnaghan EOS (Angel 2000). The errors of V_0 and K_0 are the estimated 1σ uncertainties from the EOS fit. Since the jarosite sample was probably under a semi-hydrostatic condition and because of the X-ray diffraction and loading geometry employed (the incident X-ray beam is perpendicular to the pressure loading direction and the maximum stress vector σ_1), the obtained K_0 of 55.7(1.4) GPa may represent a lower bound for the bulk modulus of jarosite.

Although both cell parameters *a* and *c* decrease with increasing pressure, their rates of contraction are quite different. As shown in Figures 3a and 3b, which are plotted at the same scale, the rate of contraction in *c* is much larger than that in *a*. Fitting the *a* and *c* data to the one-dimensional form of the Birch-Murnaghan EOS (i.e., replacing *V* with a^3 or c^3 and V_0 with a_0^3 and c_0^3 in Eq. 1) yielded a_0 = 7.306(4) Å, K_a = 104.5(4.1) GPa, and c_0 = 17.23(3) Å, K_c = 24.6(0.9) GPa. Thus a large elastic anisotropy exists between the *a* and *c* axes.

The linear compressibility (β_l) of a crystal is the relative decrease in its unit-cell length *l* when the crystal is subjected to a unit pressure and is given by

$$\beta_l = -(1/l)\,(\partial l/\partial P) = -(1/l)[1/(\partial P/\partial l)] \quad (2)$$

where *l* is the cell parameter *a* or *c* and ($\partial P/\partial a$) or ($\partial P/\partial c$) can be derived from the above fitted equations. The calculated results (Fig. 4) demonstrate large pressure dependence for β_c, whereas the variation in β_a is small. The zero-pressure compressibility of the *a* and *c* axes are 3.2×10^{-3} and 13.6×10^{-3} GPa^{-1}, respectively. Hence, the *c* axis is over four times more compressible than the *a* axis.

The anisotropic behavior of jarosite in axial compression is consistent with that in its thermal expansion. Our high-temperature neutron diffraction experiments reveal that with increasing temperature, the *c* dimension expands at a rate ~10 times larger than *a* (Xu et al. 2009), exhibiting large thermal-expansion anisotropy. Both behaviors can be explained in terms of the structure. As described earlier, the jarosite structure is composed of (001) $[Fe(O,OH)_6]/[SO_4]$ sheets that are held

TABLE 1. Unit-cell parameters of jarosite at high pressure

P (GPa)	*a* (Å)	*c* (Å)	*V* (Å^3)
0	7.299(2)	17.224(8)	794.6(5)
1.1	7.285(2)	16.984(8)	780.6(5)
2.1	7.258(3)	16.816(13)	767.2(8)
3.5	7.225(2)	16.585(7)	749.8(4)
4.7	7.208(2)	16.449(7)	740.1(4)
5.9	7.192(3)	16.308(11)	730.4(7)
6.5	7.172(4)	16.179(13)	720.7(8)
7.4	7.155(2)	16.107(8)	714.1(5)
8.1	7.139(3)	16.057(10)	708.6(6)

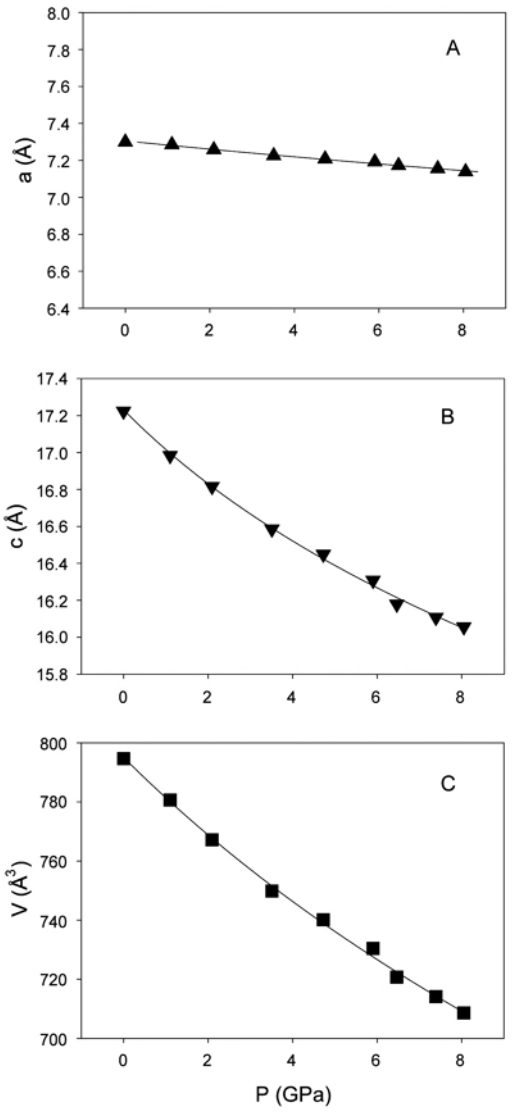

FIGURE 3. Variation of unit-cell parameters (**a**) *a*, (**b**) *c*, and (**c**) cell volume, *V*, of jarosite with pressure.

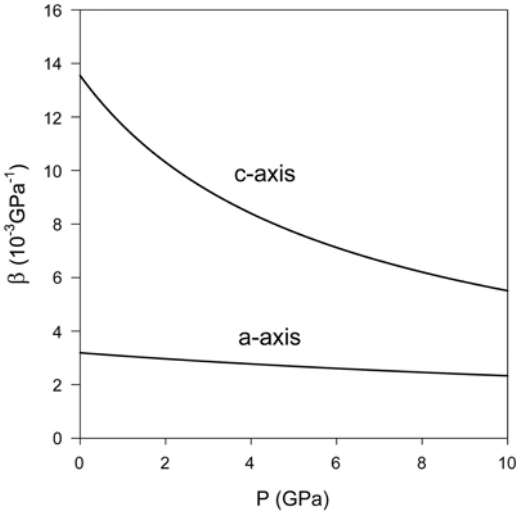

FIGURE 4. Variation of linear compressibility, β, of jarosite with pressure.

together via interstitial K^+ cations and hydrogen bonds (Fig. 1). Since the forces between the neighboring sheets are much weaker than those within the sheets themselves, the structure is more flexible along the *c* axis than in the (001) plane. More specifically, our high-temperature neutron studies show that with increasing temperature, the Fe-O3-Fe angle decreases and thus the (001) $[Fe(O,OH)_6]$ layers become more puckered via $[Fe(O,OH)_6]$ octahedral tilting, resulting in a decrease in lattice parameter *a*, but an increase in *c*. On the other hand, individual $[Fe(O,OH)_6]$ octahedra expand with increasing temperature, leading to increases in both *a* and *c*. Thus both octahedral tilting and expansion (along with S-O1 lengthening) contribute to the expansion along the *c* axis, whereas their effects largely cancel each other along *a*, resulting in large thermal-expansion anisotropy. It is expected that exerting pressure on the jarosite structure has the opposite effects, i.e., flattening the $[Fe(O,OH)_6]$ layers and contracting the $[Fe(O,OH)_6]$ octahedra. As a result, the structure contracts much more rapidly along *c* than along *a*. Hence, the *c* direction is both more compressible with pressure and more expandable with temperature.

Our determined K_0, K_a, and K_c parameters represent the first experimental measurement of bulk moduli (or compressibilities) for jarosite and its analogs (such as sodium and hydronium jarosite). Despite the deviatoric stress effect described earlier, the K_0 value (55.7 ± 1.4 GPa) is in reasonably good agreement with the K_{VRH} value (59.1 GPa) obtained by Majzlan et al. (2006) using computer simulation. These authors computed the elastic constants of jarosite from the interatomic potentials of Becker and Gasharova (2001) using the GULP code (Gale 1997). The calculated Voigt (K_V) and Reuss (K_R) bounds of the bulk modulus are 72.1 and 46.1 GPa, respectively, giving an average value (K_{VRH}) of 59.1 GPa. As stated by these authors, these calculated elastic parameters are only predictions whose uncertainties are unknown. Nevertheless, the agreement between our measured K_0 and the calculated K_{VRH} indicates the general validity of the GULP approach and of the interatomic potentials used. On the other hand, our measured zero-pressure linear compressibilities β_a (3.2×10^{-3} GPa^{-1}) and β_c (13.6×10^{-3} GPa^{-1}) are somewhat different from those calculated using the same model. According to Nye (1998), the linear compressibilities of a trigonal crystal are related to its elastic compliances s_{ij} as follows:

$$d(a/a_0)/dP = s_{11} + s_{12} + s_{13} \quad (3)$$
$$d(c/c_0)/dP = 2s_{13} + s_{33}. \quad (4)$$

The calculated $d(a/a_0)/dP$ and $d(c/c_0)/dP$ from the s_{ij} values of Majzlan et al. (2006) are 2.157×10^{-3} and 17.378×10^{-3} GPa^{-1}, respectively. Thus the calculated linear compressibility β_a is smaller than our measured β_a (3.2×10^{-3} GPa^{-1}), whereas the calculated β_c is larger than the measured value (13.6×10^{-3} GPa^{-1}). Hence, the simulation model significantly underestimates β_a and overestimates β_c. As the underestimation in β_a and the overestimation in β_c approximately compensate for each other, the calculated volume compressibility (or bulk modulus) is in reasonably good agreement with our measured value.

Majzlan et al. (2006) measured the elastic properties of alunite, $KAl_3(SO_4)_2(OH)_6$, using Brillouin spectroscopy. Alunite is isostructural with jarosite, but has a smaller unit-cell volume (724.08 $Å^3$ compared with 791.3 $Å^3$ for jarosite) due to the smaller Al^{3+} compared with Fe^{3+}. The bulk modulus (the K_{VRH} value from Majzlan et al. 2006) of alunite is 62.6 ± 0.7 GPa, which is larger than our measured 56.0 ± 1.3 GPa for jarosite. This is consistent with the well-known inverse relation between bulk modulus and ambient cell volume for isostructural compounds (e.g., Anderson and Anderson 1970). Apparently, the longer (and weaker) Fe-O bonds (Fe-O2 = 2.0501 Å and Fe-O3 = 1.9815 Å in jarosite) are more compressible than Al-O (Al-O2 = 1.9510 Å and Al-O3 = 1.8743 Å in alunite), resulting in the smaller bulk modulus for jarosite. To determine the detailed compressibility systematics in jarosite and the associated alunite group, however, more compositions need to be studied.

ACKNOWLEDGMENTS

We thank J. Majzlan for helpful suggestions and R. Peterson and an anonymous reviewer for constructive reviews. Use of the National Synchrotron Light Source, Brookhaven National Laboratory, was supported by the U.S. Department of Energy, Office of Science, Office of Basic Energy Sciences, under contract no. DE-AC02-98CH10886. Use of the X17B2 beamline was supported by COMPRES, the Consortium for Materials Properties Research in Earth Sciences under NSF Cooperative Agreement EAR 01-35554 and by the Mineral Physics Institute, Stony Brook University. Los Alamos National Laboratory is operated by Los Alamos National Security, LLC, under DOE contract DE-AC52-06NA25396.

REFERENCES CITED

Anderson, D.L. and Anderson, O.L. (1970) The bulk modulus-volume relationship for oxides. Journal of Geophysical Research, 75, 3494–3500.

Angel, R.J. (2000) Equation of state. In R.M. Hazen and R.T. Downs, Eds., High-Temperature and High-Pressure Crystal Chemistry, 41, p. 35–59. Reviews in Mineralogy and Geochemistry, Mineralogical Society of America, Chantilly, Virginia.

Ballhorn, R., Brunner, H., and Schwab, R.G. (1989) Artificial compounds of the crandallite type: a new material for separation an immobilization of fission products. Scientific Basis for Nuclear Waste Management, 12, 249–252.

Basciano, L.C. and Peterson, R.C. (2007) Jarosite-hydronium jarosite solid-solution series with full iron site occupancy: Mineralogy and crystal chemistry. American Mineralogist, 92, 1464–1473.

Becker, U. and Gasharova, B. (2001) AFM observations and simulations of jarosite growth at the molecular scale: Probing the basis for the incorporation of foreign ions into jarosite as a storage mineral. Physics and Chemistry of Minerals, 28, 545–556.

Birch, F. (1952) Elasticity and constitution of the Earth's interior. Journal of

Geophysical Research, 57, 227–286.
Decker, D.L. (1971) High-pressure equation of state for NaCl, KCl, and CsCl. Journal of Applied Physics, 42, 3239–3244.
Drouet, C. and Navrotsky, A. (2003) Synthesis, characterization, and thermochemistry of K-Na-H_3O jarosites. Geochimica et Cosmochimica Acta, 67, 2063–2076.
Dutrizac, J.E. and Jambor, J.L. (2000) Jarosite and their application in hydrometallurgy. In C.N. Alpers and J.L. Jambor, Eds., Sulfate Minerals: Crystallography, Geochemistry, and Environmental Significance, 40, p. 405–452. Reviews in Mineralogy and Geochemistry, Mineralogical Society of America, Chantilly, Virginia.
Gale, J.D. (1997) GULP: A computer program for the symmetry-adapted simulation of solids. Journal of the Chemical Society, Faraday Transactions, 93, 629–637.
Glasnak, P. and Majzlan, J. (2007) Single crystal X-ray refinement and thermodynamic properties of stoichiometric jarosite, $KFe_3(SO_4)_2(OH)_6$. Geochimica et Cosmochimica Acta, Supplement, 71, A327.
Grohol, D., Nocera, D.G., and Papoutsakis, D. (2003) Magnetism of pure iron jarosites. Physical Review B, 67, 064401.
Inami, T., Nishiyama, M., Meegawa, S., and Oka, Y. (2000) Magnetic structure of the *kagomé* lattice antiferromagnet potassium jarosite $KFe_3(OH)_6(SO_4)_2$. Physical Review B, 61, 12181–12186.
Klingelhöfer, G., Morris, R.V., and others (2004) Jarosite and hematite at Meridiani Planum from Opportunity's Mössbauer spectrometer. Science, 306, 1740–1745.
Kolitsch, U., Tiekink, E.R.T., Slade, P.G., Taylor, M.R., and Pring, A. (1999) Hinsdalite and plumbogummite, their atomic arrangements and disordered lead sites. European Journal of Mineralogy, 11, 513–520.
Kotler, J.M., Hinman, N.W., Yan, B., Stoner, D.L., and Scott, J.R. (2008) Glycine identification in natural jarosites using laser desorption Fourier transform mass spectrometry: Implications for the search for life on Mars. Astrobiology, 8, 253–266.
Majzlan, J., Speziale, S., Duffy, T.S., and Burns, P.C. (2006) Single-crystal elastic properties of alunite, $KAl_3(SO_4)_2(OH)_6$. Physics and Chemistry of Minerals, 33, 567–573.
Menchetti, S. and Sabelli, C. (1976) Crystal chemistry of the alunite series: Crystal structure refinement of alunite and synthetic jarosite. Neues Jahrbuch für Mineralogie, Monatshefte, 406–417.
Navrotsky, A., Forray, F.L., and Drouet, C. (2005) Jarosite stability on Mars. Icarus, 176, 250–253.
Nye, J.F. (1998) Physical Properties of Crystals—Their representation by tensors and matrices, 329 p. Clarendon Press, Oxford.
Papike, J.J., Karner, J.M., and Shearer, C.K. (2006) Comparative planetary mineralogy: Implications of Martian and terrestrial jarosite. A crystal chemical perspective. Geochimica et Cosmochimica Acta, 70, 1309–1321.
Stoffregen, R.E., Alpers, C.N., and Jambor, J.L. (2000) Alunite-jarosite crystallography, thermodynamics, and geochronology. In C.N. Alpers, J.L. Jambor, Eds., Sulfate Minerals: Crystallography, Geochemistry, and Environmental Significance, 40, p. 453–479. Reviews in Mineralogy and Geochemistry, Mineralogical Society of America, Chantilly, Virginia.
Weidner, D.J., Vaughan, M.T., Ko, J., Wang, Y., Liu, X., Yeganeh-Haeri, A., Pacalo, R.E., and Zhao, Y. (1992) Characterization of stress, pressure and temperature in SAM85, a DIA type high pressure apparatus. In Y. Syono and M.H. Manghnani, Eds., High Pressure Research: Application to Earth and Planetary Sciences, 67, p. 13–17. Geophysics Monograph Series, American Geophysical Union, Washington, D.C.
Weidner, D.J., Wang, Y., and Vaughan, M.T. (1994) Yield strength at high pressure and temperature. Geophysical Research Letters, 21, 753–756.
Wills, A.S., Harrison, A., Ritter, C., and Smith, R.I. (2000) Magnetic properties of pure and diamagnetically doped jarosites: Model *kagomé* antiferromagnets with variable coverage of the magnetic lattice. Physical Review B, 61, 6156–6169.
Xu, H., Zhao, Y., Vogel, S.C., Hickmott, D.D., Daemen, L.L., and Hartl, M.A. (2009) Thermal expansion and decomposition of jarosite: a high-temperature neutron diffraction study. Physics and Chemistry of Minerals, in press, DOI: 10.1007/s00269-009-0311-5.
Yildirim, T. and Harris, A.B. (2006) Magnetic structure and spin waves in the Kagomé jarosite compound $KFe_3(SO_4)_2(OH)_6$. Physical Review B, 73, 214446.
Zhao, Y. and Zhang, J. (2008) Microstrain and grain-size analysis from diffraction peak width and graphical derivation of high-pressure thermomechanics. Journal of Applied Crystallography, 41, 1095–1108.

Manuscript received April 28, 2009
Manuscript accepted September 1, 2009
Manuscript handled by Guoyin Shen